Cureus
Part of SPRINGER NATURE

Open Access Case Report

# Nonimmune Hydrops and Arthrogryposis Associated With a Homozygous GPR107 Gene Splice Site Variant

**Review began** 10/12/2026
**Review ended** 11/15/2026
**Published** 11/16/2026

**© Copyright** 2026
Pradhan et al. This is an open access article distributed under the terms of the Creative Commons Attribution License CC-BY 4.0., which permits unrestricted use, distribution, and reproduction in any medium, provided the original author and source are credited.

**DOI:** 10.7759/cureus.119761

Mandakini Pradhan [1], Kritika Agnihotri [1], Arnav Asher [2], Tushar Kachhadiya [3], Shwetal Patel [3], Shalin Vaniawala [3], Salil Vaniawala [3], Pramila Menon [4], Vasundhara Tamhankar [2, 3], Parag M. Tamhankar [3, 2, 4]

1. Fetal Medicine, Sanjay Gandhi Post Graduate Institute of Medical Sciences, Lucknow, IND 2. Genetics, Centre for Medical Genetics, Mumbai, IND 3. Genetics, SN Gene Lab Pvt Ltd, Surat, IND 4. Pediatrics, Dr. D.Y. Patil Medical College, Hospital and Research Centre, Dr. D.Y. Patil Vidyapeeth, Pimpri, Pune, IND

**Corresponding author:** Mandakini Pradhan, mpradhan9918@gmail.com

## Abstract

*GPR107* is a G protein-coupled receptor (GPCR) primarily involved in intracellular trafficking and retrograde transport, particularly in the Golgi-to-endoplasmic reticulum (ER) pathway. *GPR107* is also expressed in various tissues and may play a role in cell signaling and gene expression regulation. Experimental deletion of *Gpr107* in mice has been shown to lead to an embryonic lethal phenotype that is characterized by a reduction in cubilin transcript abundance and a decrease in the representation of multiple genes implicated in the cubilin-megalin endocytic receptor complex. No human phenotype has been reported yet in association with this gene. Herein, we report a fetus born of a third-degree consanguineous marriage having non-immune hydrops, fetal akinesia, and a homozygous near-splice variant in the *GPR107* gene ([GRCh38] chr9:g.130104417T>G or c.1132-3T>G), identified on exome sequencing. Parental exome sequencing showed them to be carriers of the same variant. Sanger sequencing confirmed homozygosity in the fetus and heterozygosity in both parents. The couple had a history of a similarly affected baby, leading to in utero death at seven months' gestation. The variant c.1132-3T>G is predicted to lead to loss of function by affecting the splicing mechanism. In the absence of functional studies, the variant remains a variant of uncertain significance, and *GPR107* is proposed as a candidate gene for this phenotype.

**Categories:** Obstetrics/Gynecology, Radiology, Genetics
**Keywords:** arthrogryposis, exome sequencing, gpr107, hydrops fetalis, splice-site variant

## Introduction

Fetal akinesia, or arthrogryposis multiplex congenita (arthron = joint), is a condition that consists of contractures affecting two or more joints prenatally. Incidence is one in 3000 live births; however, the antenatal incidence may be higher, implying high mortality. This syndrome is also known as the fetal akinesia deformation sequence. Additional features include hydrops, intrauterine growth retardation, facial anomalies, skin pterygia, hypoplastic palmar dermal ridges, hypoplastic lungs, and polyhydramnios. Etiology can be primary due to mutations in chromosomes or genes, or secondary due to extrinsic etiology leading to in utero crowding such as oligohydramnios, uterine abnormalities, and twin pregnancies. Chromosomal disorders include trisomy 18 or trisomy 8. Single-gene etiologies involve mutations in any of the approximately 90 genes, including *RAPSN, DOK7, MUSK, CHRNA1, CHRND, CHRNG*, and others [1,2].

Hydrops fetalis is defined as excessive, pathologic fluid accumulation within two or more tissues or body cavities, including the peritoneal cavity, pleural space, pericardial sac, and skin. Immune hydrops fetalis, also known as erythroblastosis fetalis, occurs in the setting of hemolytic disease of the fetus and newborn (HDFN), which can lead to severe anemia. Nonimmune hydrops fetalis may result from a wide range of underlying etiologies, including cardiac abnormalities, chromosomal aneuploidy, hemoglobinopathies, lymphatic malformations, lysosomal storage diseases, congenital anemias, and congenital infections, among others [3,4].

*GPR107* encodes an orphan G protein-coupled receptor (orphan GPCR)-like protein of the LUSTR family that resides mainly in the trans-Golgi network (TGN) and takes part in clathrin-mediated endocytosis (CME), receptor recycling, and retrograde transport from endosomes and the Golgi apparatus to the endoplasmic reticulum [5-7]. Mice with disruption of the *Gpr107* locus die during embryonic development, indicating that the gene is essential for normal development [7,8]. Exome sequencing analyzes the protein-coding exons and the adjoining intronic sequences of almost all genes in a single test. A near-splice variant is an intronic change that lies close to, but outside, the invariant AG or GT dinucleotides of an exon-intron boundary (for example, at positions −3 to −20 of an acceptor site); such variants can weaken the splice site and lead to exon skipping or the use of cryptic splice sites [9]. A variant of uncertain significance (VUS) is a variant for which the available evidence is insufficient to classify it as pathogenic or benign under the American College of Medical Genetics and Genomics/Association for Molecular Pathology (ACMG/AMP) guidelines [10]. In

autosomal recessive inheritance, an affected individual carries disease-causing variants on both copies of a gene, each parent is usually a healthy heterozygous carrier, and the recurrence risk is 25% in each pregnancy; parental consanguinity increases the chance that both parents carry the same rare variant.

Herein, we report for the first time a fetus born of a third-degree consanguineous marriage having non-immune hydrops, fetal akinesia/ arthrogryposis multiplex congenita, associated with a homozygous near-splice variant in the *GPR107* gene (chr9:g.130104417T>G or c.1132-3T>G), identified on exome sequencing. Asymptomatic parents were identified to be heterozygous for the same variant on exome sequencing, and this was confirmed by Sanger sequencing, suggesting an autosomal recessive inheritance pattern. No human phenotype has been previously reported for *GPR107* gene deficiency, as per our search in the medical literature and available databases, including PubMed/MEDLINE (Medical Literature Analysis and Retrieval System Online) and Google Scholar.

## Case Presentation

A third-degree consanguineous couple presented in their second pregnancy for counseling and fetal anomaly detection by ultrasound (USG) in their second trimester. The mother was 25 years old, and the father was 23 years old. There was no history of maternal gestational diabetes, pregnancy-induced hypertension, or exposure to teratogenic agents during the pregnancy. Fetal two-dimensional/three-dimensional USG showed a biparietal diameter of 5.75 cm (corresponding to 23 weeks 4 days), head circumference of 23.5 cm (25 weeks 4 days), abdominal circumference of 19.68 cm (24 weeks 2 days), femur length of 3.51 cm (21 weeks 1 days), tibia length of 3.1 cm (21 weeks 3 days), fibula length of 2.9 cm (20 weeks 2 days), humerus length of 3.52 cm (22 weeks 1 days), radius length of 3.21 cm (23 weeks), ulnar length of 3.24 cm (22 weeks 3 days), and transcerebellar diameter of 2.14 cm (20 weeks 3 days). The mean gestational age was 23 weeks. Amniotic fluid was normal (maximum vertical pocket 6.16 cm); there was no polyhydramnios. The fetus showed signs of hydrops: generalized skin edema, bilateral pleural effusion, ascites, and scalp edema. The fetus also showed signs of fetal akinesia/arthrogryposis multiplex congenita: hyperextended neck, persistently flexed hips and knees, talipes equinovarus. The fetus maintained persistently clenched fists during the scan, and no spontaneous movements of the trunk or limbs were observed during real-time scanning (Figure *1*, Figure *2*, Figure *3*, and Video *1*).

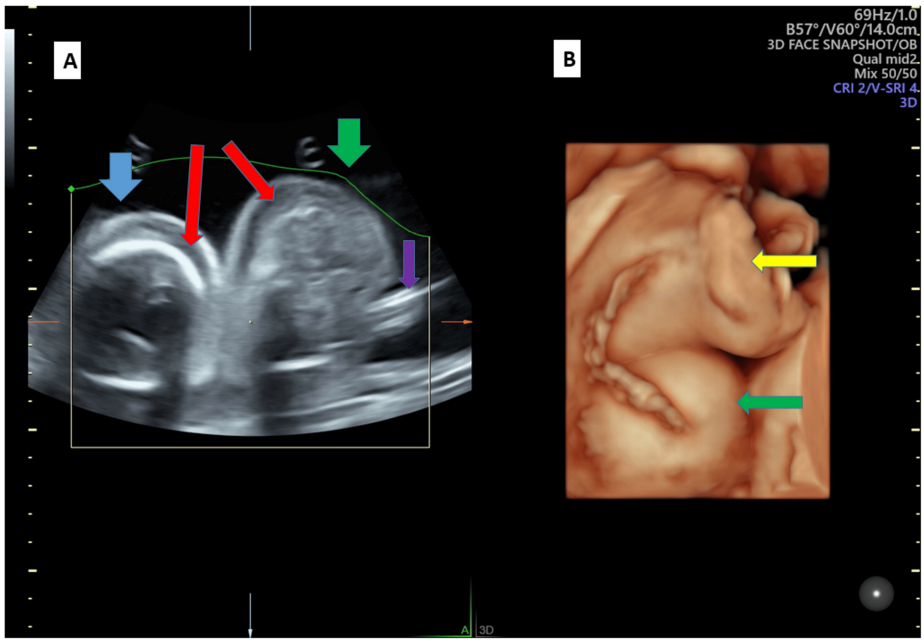



**FIGURE 1: Fetal ultrasound image in the second trimester of pregnancy showing subcutaneous edema, pleural effusion, ascites, and flexed posture of the torso**

Fetal ultrasound image in the second trimester of pregnancy (mean sonographic gestational age 23 weeks). On the left side (A), we see a two-dimensional image showing a section of the thorax (blue arrow) and abdomen (green arrow) in the same section because the baby is in a flexed posture. Subcutaneous fluid collections are seen (red arrows) in the thorax and abdomen, suggestive of hydrops fetalis; a normal cord (purple) is seen attached to the abdomen. On the right side (B), we see a three-dimensional surface rendering of the section seen in A, with fixed, flexed lower limbs suggesting arthrogryposis (yellow arrow) and the abdomen (green arrow) seen.

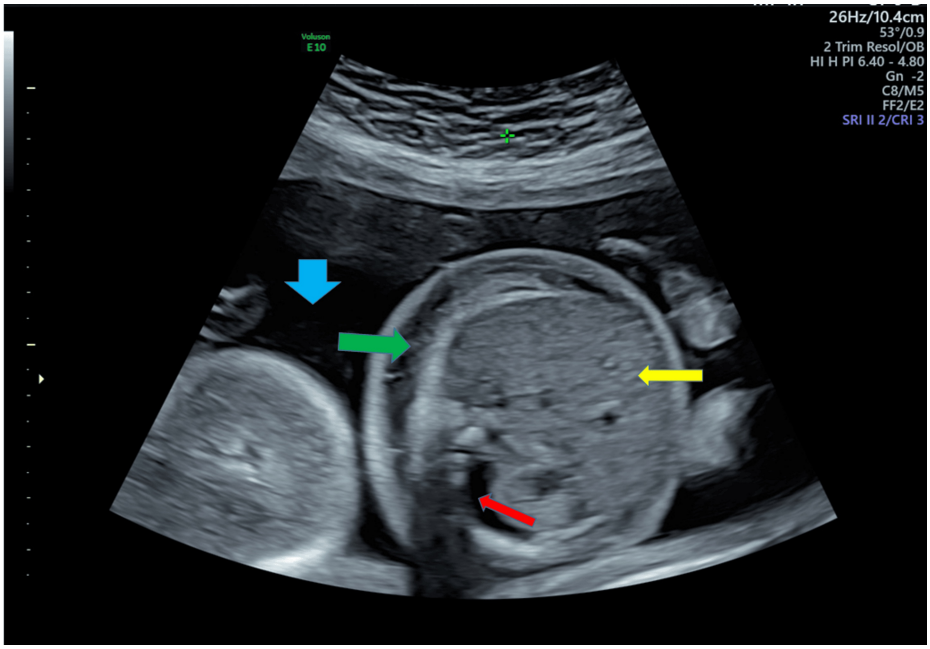



**FIGURE 2: Fetal ascites and abdominal subcutaneous edema seen in two-dimensional ultrasound in the second trimester of pregnancy**

Two-dimensional ultrasound image of the fetus in the second trimester of pregnancy (mean sonographic gestational age 23 weeks), showing a section of the abdomen with subcutaneous fluid collection (green arrow), ascites (red arrow), and liver (yellow arrow) seen in the image. Amniotic fluid (blue arrow) was adequate.

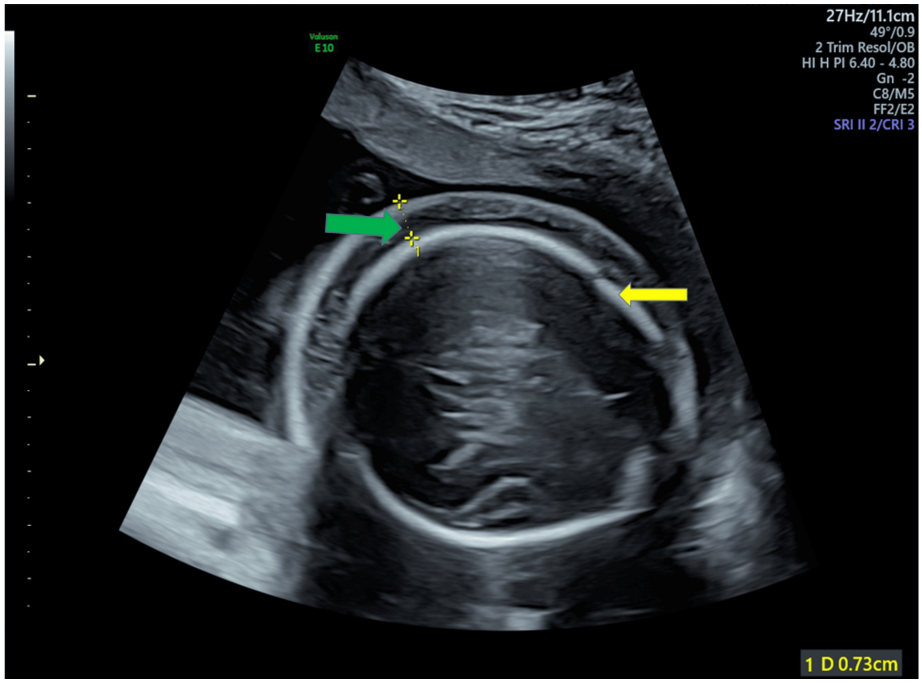



**FIGURE 3: Fetal scalp edema seen in two-dimensional ultrasound in the second trimester of pregnancy**

Two-dimensional ultrasound image of the second-trimester fetus (mean sonographic gestational age 23 weeks), showing a section of the head (yellow arrow) with scalp edema (green arrow) and normal intracranial anatomy.




**VIDEO 1: Antenatal ultrasonographic evaluation demonstrating features of hydrops fetalis and fetal akinesia deformation sequence**

Real-time two-dimensional ultrasonographic sweep of the fetus. The initial cross-sectional view shows significant persistent flexion posture across the fetal torso with marked diffuse subcutaneous tissue edema, ascites, and pleural effusion. Sequential inferior scanning across the pelvis and lower extremities reveals hyperflexed, rigid positioning of the lower limbs and feet within clear amniotic fluid, displaying an absence of spontaneous movements indicative of fetal akinesia. Concluding sweep across the chest and abdomen reconfirms generalized body wall edema and severe fluid collection characteristic of non-immune hydrops fetalis.

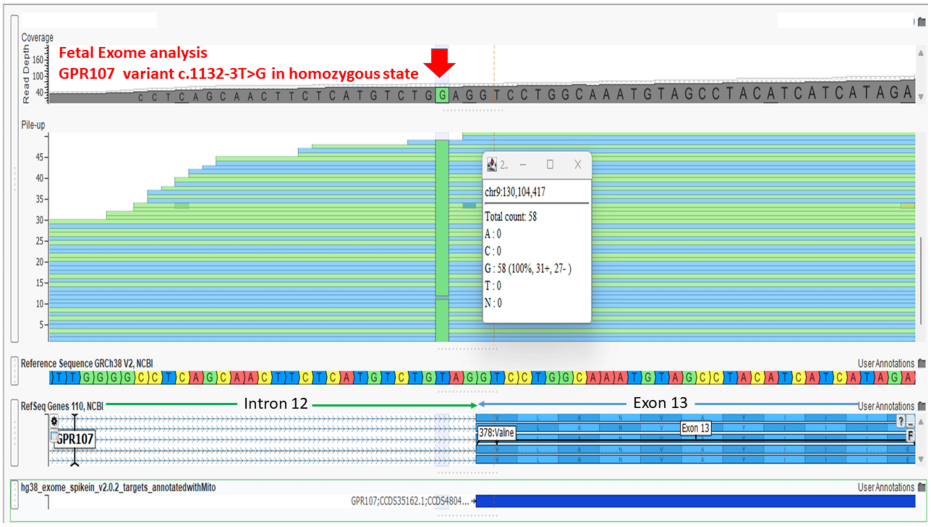
View video here: https://www.youtube.com/watch?v=o_fPbs8heJI

Fetal two-dimensional echocardiography was normal, and we documented no other fetal anomalies apart from those described above.

Using Human Phenotype Ontology (HPO) terms [11], the fetal phenotype comprised hydrops fetalis (HP:0001789), generalized edema (HP:0007430), pleural effusion (HP:0002202), ascites (HP:0001541), arthrogryposis multiplex congenita (HP:0002804), fetal akinesia sequence (HP:0001989), decreased fetal movement (HP:0001558), hip contracture (HP:0003273), knee flexion contracture (HP:0006380), talipes equinovarus (HP:0001762), and hand clenching (HP:0001188).

The pregnancy was terminated at 23 weeks of gestation, and post-termination examination confirmed hydrops and arthrogryposis multiplex congenita (photos not available) in a male fetus. The couple had a previous pregnancy with a similarly affected female baby with in utero death around seven months' gestation. Details about this pregnancy were not available.

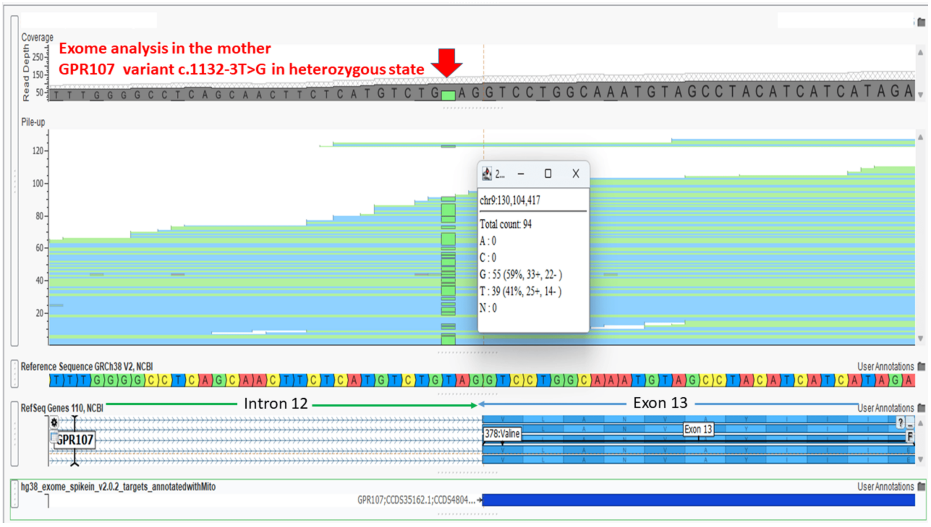
Genetic counseling was performed, and an autosomal recessive genetic condition was suspected owing to consanguinity and two fetuses of opposite sex being affected by the same condition. Amniotic fluid obtained by amniocentesis was sent for fetal genetic testing, and ethylenediaminetetraacetic acid (EDTA) peripheral blood samples were collected from both parents. Chromosomal microarray showed normal results. The Next Generation Sequencing (NGS) analysis was performed using targeted capture-based library preparation from amniotic fluid or other clinical specimens. Sequencing was conducted on the Illumina NovaSeq 6000 platform using Paired-End 2X150 chemistry. The bioinformatics pipeline followed the standard GATK best practices framework, with sequence reads assembled and aligned to the human reference genome build GRCh38 based on NCBI RefSeq transcripts. Variant identification for single-nucleotide variants (SNVs) and small insertions/deletions (Indels) was executed via HaplotypeCaller, while copy number variants (CNVs) were called using read-depth comparison against a matched reference dataset with a sensitivity of 70-75% using ExomeDepth (version 1.1.10) [12,13]. Variant filtering and classification adhered strictly to American College of Medical Genetics guidelines [10], leveraging population databases including 1000Genomes, Exome Aggregation Consortium database (ExAC), Genome Aggregation database (gnomAD), and Single Nucleotide Polymorphism database (dbSNP), alongside in silico prediction tools such as PolyPhen-2, Sorting Intolerant from Tolerant (SIFT), and MutationTaster2 [14-20]. The sequencing assay spanned a total of 20,321 exome genes, including 37 mitochondrial genes (Twist exome panel 2.0 with additional mitochondrial gene coverage added; Twist Biosciences Inc., South San Francisco, CA, USA). Exome sequencing in the fetus generated a total yield of 7.74 Gb of data. High-quality data was demonstrated by a Q30 base score rate of 93.70% and a read alignment rate of 99.47% out of 100% of total generated reads. For the mother, the exome sequencing assay yielded a total of 12.3 Gb of sequencing data. Her sample demonstrated high data quality with 93.19% of bases scoring above Q30 and achieved an alignment rate of 99.52% out of 100.00% total reads. For the husband, the exome sequencing assay generated 10.5 Gb of total data, with 93.37% of bases exceeding the Q30 quality threshold and an alignment rate of 99.49% out of 100.00% total reads. All three runs successfully fulfilled the target mean coverage requirement of >85-100x across the targeted exonic regions. The lab has been accredited by the National Accreditation Board for Testing and Calibrating Laboratories (NABL) of India. The fetus was identified to be homozygous for a novel variant in the *GPR107* gene with genomic coordinates chr9:g.130104417T>G (GRCh38 format) or c.1132-3T>G (transcript ID NM_020960.5) (read depth: 31x) (located in intron 12) and affecting the acceptor splice site between intron 12 and exon 13 (Figure *4*).




## FIGURE 4: Whole-exome sequencing analysis of the affected fetus confirming the GPR107 homozygous variant

Integrative Genomics Viewer (VarSeq, Golden Helix) screenshot of the binary alignment map (BAM) file derived from fetal whole-exome sequencing data. Visual alignment displays the homozygous splice-site variant chr9:g.130104417T>G (corresponding to c.1132-3T>G) within intron 12 of the *GPR107* gene (indicated by the red arrow), with 100% read depth coverage for the mutant allele (n=58). The viewer counts all aligned reads; the filtered read depth reported by the variant caller was 31x).

Exome sequencing performed for the couple confirmed them to be heterozygous for the same variant (read depth of the nucleotide c.1132-3 in the mother was 64x/variant allele frequency (VAF) being 56%, and read depth in the father was 54x/VAF being 48%), suggesting an autosomal recessive inheritance (Figure *5*, Figure *6*).




## FIGURE 5: Whole-exome sequencing analysis of the mother confirming the heterozygous state of the GPR107 variant

Integrative Genomics Viewer (VarSeq, Golden Helix) screenshot of the binary alignment map (BAM) file derived from the mother's whole-exome sequencing data. Visual alignment demonstrates the heterozygous splice-site variant chr9:g.130104417T>G (c.1132-3T>G) within intron 12 of the *GPR107* gene (indicated by the red arrow) with a total read depth count of 94, showing an allele distribution of 59% (n=55) for the mutant G allele and 41% (n=39) for the wild-type T allele. The viewer counts all aligned reads; the filtered read depth reported by the variant caller was 64x (variant allele frequency 56%).

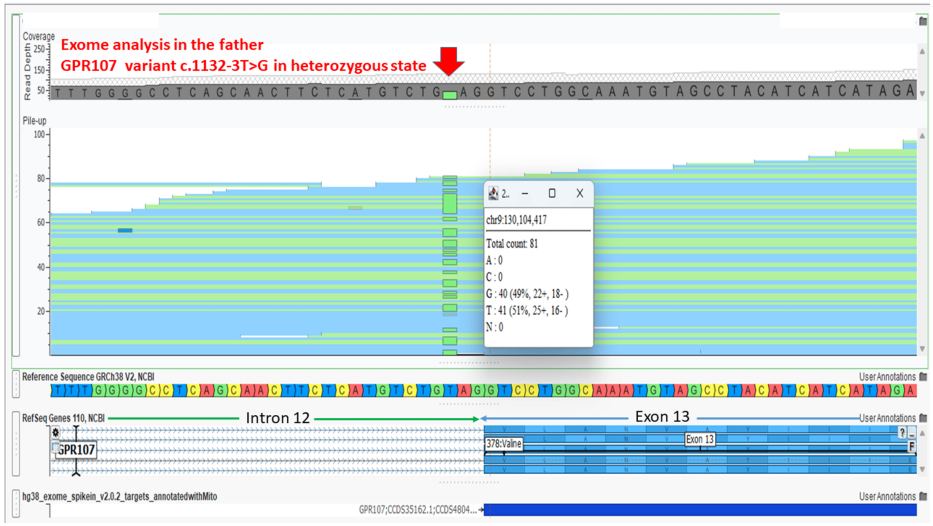



**FIGURE 6: Whole-exome sequencing analysis of the father confirming the heterozygous state of the GPR107 variant**

Integrative Genomics Viewer (VarSeq, Golden Helix) screenshot of the binary alignment map (BAM) file derived from the father's whole-exome sequencing data. The visual alignment demonstrates the heterozygous splice-site variant chr9:g.130104417T>G (c.1132-3T>G) within intron 12 of the *GPR107* gene (indicated by the red arrow), with a total read depth count of 81, showing an allele distribution of 49% (n=40) for the mutant G allele and 51% (n=41) for the wild-type T allele. The viewer counts all aligned reads; the filtered read depth reported by the variant caller was 54x (variant allele frequency 48%).

The read depths and variant allele frequencies given in the text (fetus 31x/100%, mother 64x/56%, father 54x/48%) are those reported by the variant caller, which counts only reads that pass its quality filters (for example, after removal of duplicate and low-quality reads). The higher read counts shown in Figures *4*-*6* (58, 94, and 81, respectively) are all aligned reads displayed at this position in the alignment viewer. Both measures give the same genotypes, with similar allele fractions in the parents.

## Sanger sequencing

The variant and its segregation were confirmed by bidirectional Sanger (dideoxy chain-termination) sequencing [21]. A fragment spanning the intron 12-exon 13 junction of *GPR107* (NM_020960.5) was amplified by polymerase chain reaction (PCR) from the same genomic DNA samples that had been used for exome sequencing, namely DNA extracted from amniotic fluid for the fetus and from EDTA peripheral blood for each parent (the laboratory case identifiers of the Sanger and exome samples were matched), using locus-specific primers flanking c.1132-3 (primer sequences and PCR conditions are available from the authors on request). The PCR products were purified and sequenced in the forward and reverse directions using BigDye Terminator v3.1 cycle sequencing chemistry (Applied Biosystems, Thermo Fisher Scientific, Waltham, MA, USA). The purified extension products were separated by capillary electrophoresis on a 3500 Dx Genetic Analyzer with POP-7 polymer (Applied Biosystems), and bases were called with the KB Basecaller (version 1.4.1.8). The electropherograms were inspected visually and compared with the reference sequence (GRCh38; NM_020960.5) at the variant position.

Sanger sequencing confirmed that the fetus was homozygous for c.1132-3T>G, showing a single G peak at position c.1132-3, whereas both parents showed overlapping T and G peaks of similar height at this position, consistent with heterozygosity (Figure *7*). In the reverse-direction reads, the variant lay close to the sequencing primer, within the early low-resolution part of the read, so genotypes were assigned from the high-quality forward reads. These results confirm the exome sequencing findings and the segregation of the variant in an autosomal recessive pattern in this family (Figure *7*).




**FIGURE 7: Sanger sequencing confirming the GPR107 c.1132-3T>G variant in the fetus (homozygous) and both parents (heterozygous)**

Forward-strand electropherograms spanning the intron 12-exon 13 junction of *GPR107* (NM_020960.5). (A) The fetus shows a single G peak at c.1132-3 (shaded column, arrowhead), consistent with homozygosity for c.1132-3T>G. (B) The mother and (C) the father show overlapping T (red) and G (black) peaks of similar height at the same position (IUPAC code K = G/T), consistent with heterozygous carrier status. The dashed line marks the intron 12/exon 13 boundary; the AG dinucleotide of the acceptor site lies immediately downstream of the variant. Peak colors: A, green; C, blue; G, black; T, red. Peak heights (relative fluorescence units) at c.1132-3: fetus G 1042/T 3; mother G 630/T 544; father G 664/T 471.

Figure credit: Generated by the authors from the original sequencing trace files.

Franklin online software predicted the variant to be deleterious by affecting the splicing mechanism [22]. As per Franklin analysis, the variant was absent in the gnomAD database, GenomeAsia, India DB, Mexican DB, Iranome, TOPMed Bravo, GME Variome, Turkish Variome, 4.7KJPN, 1000Genomes, ExAC, ESP 6500, ABraOM, and SN Gene Lab internal exome database [22]. The aggregate prediction by Franklin listed in silico tools was deleterious (score 0.78) [22]. Splice-altering tool scores were given as follows: Splice AI - splice altering/strong (score 0.89), dbsc SNV Ada - deleterious (0.9), dbscSNV RF - deleterious (0.72). Other in silico tools were given as not applicable (since it was an intronic variant): conservation (GERP), functional coding (Revel, AlphaMissense, Eve, Varity, MUT Assessor, SIFT, PolyPhen2, MutationTaster, FATHMM, DANN, MetaLR, PrimateAI, BayesDel, CardioBoost ARM, CardioBoost CM), functional whole genome tools (GenoCanyon, fitCons), and mitochondrial (MitoTip, APOGEE) [22]. As per Franklin, the ACMG classification suggested for this variant was VUS (PM2_moderate - the variant is absent in all databases, and PP3 - computational tools unanimously predict a deleterious effect on the gene) [22].

## Splicing impact and computational prediction summary

The potential effect of the *GPR107* gene variant NM_020960.5:c.1132-3T>G (chr9:130104417 T>G, GRCh38/hg38) on pre-mRNA splicing was assessed using SpliceAI Lookup [23]. The analysis used the GRCh38 genome built with the basic GENCODE transcript annotation, a maximum scoring distance of 500 bp, and unmasked scores. SpliceAI is a deep-learning model that predicts the probability of each position being a splice acceptor or donor, and reports delta scores (0 to 1) for acceptor gain, acceptor loss, donor gain,

and donor loss relative to the reference sequence [24]. Pangolin, a deep-learning model that predicts splice site usage, was run in parallel and reports splice gain and splice loss scores [25]. Delta scores of ⩾0.5 were considered supportive of a splicing alteration (the ClinGen Sequence Variant Interpretation Splicing Subgroup uses a SpliceAI score of ⩾0.2 as the threshold for supporting computational evidence of a splicing effect [9]). The predicted splicing consequence and its effect on the encoded protein were obtained with the SpliceAI-10k calculator, which infers the likely aberrant transcript (e.g., exon skipping, intron retention, cryptic site use) and its impact on the reading frame [26]. The MANE Select transcript (ENST00000347136.11/NM_020960.5) was used for all analyses. Results of the in silico prediction of the splicing effect of *GPR107* c.1132-3T>G: The variant c.1132-3T>G lies at the −3 position of the intron 12 acceptor splice site of *GPR107*, within the polypyrimidine tract immediately upstream of exon 13. SpliceAI predicted a strong loss of the canonical acceptor site (Δ score 0.89; 3 bp from the variant) and of the exon 13 donor site (Δ score 0.71; 133 bp from the variant). Scores for acceptor gain (0.11) and donor gain (0.00) were low, indicating that activation of a cryptic splice site is unlikely. Pangolin independently predicted splice loss at the same position (Δ score 0.79; 3 bp) with a low splice gain score (0.12). The SpliceAI-10k calculator predicted that loss of the exon 13 acceptor results in skipping of exon 13 (131 bp of coding sequence). Because 131 is not divisible by three, this is predicted to cause a frameshift, producing the protein change p.(Leu379Asnfs*17). The resulting transcript is predicted to encode a truncated protein of 394 amino acids with an altered C-terminal sequence, compared with the 552-amino-acid wild-type protein. The aberrant transcript is also expected to be a candidate for nonsense-mediated mRNA decay because, in the exon 13-skipped transcript, the predicted premature termination codon lies in exon 15, more than 200 nucleotides upstream of the last exon-exon junction (exon 17/exon 18), well beyond the 50-55 nucleotide boundary for nonsense-mediated decay. Together, these predictions suggest that c.1132-3T>G is likely to impair normal splicing and result in loss of function of *GPR107*. Additionally, the AlphaGenome Variant Impact (AVI) tool assigns this variant a score of 25.25, placing its overall predicted functional severity within the top 0.3% of all SNVs (very high functional impact on the gene and its product) (Figure *8*).

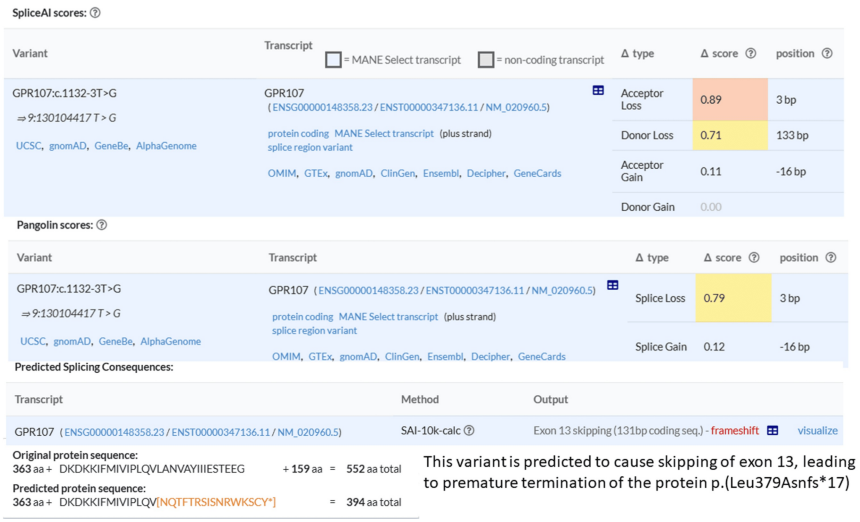



**FIGURE 8: In silico splicing analysis of the GPR107 variant c.1132-3T>G (NM_020960.5; chr9:130104417 T>G, GRCh38) using SpliceAI and Pangolin in silico tools**

SpliceAI Lookup (Broad Institute) predicts that the *GPR107* gene variant, located at the −3 position of the intron 12 acceptor splice site, disrupts normal splicing. SpliceAI delta scores indicate a high probability of acceptor loss (Δ score 0.89, 3 bp from the variant) and donor loss (Δ score 0.71, 133 bp from the variant), with low scores for acceptor gain (0.11, −16 bp) and donor gain (0.00). Pangolin independently predicts splice loss (Δ score 0.79, 3 bp) and a low splice gain score (0.12, −16 bp). The predicted splicing consequence (SAI-10k-calc) is skipping of exon 13 (131 bp of coding sequence), causing a frameshift. At the protein level, this is predicted to result in the substitution p.(Leu379Asnfs*17), leading to premature termination. The original 552 aa protein is predicted to be truncated to 394 aa, with the altered C-terminal sequence shown in orange. Scores range from 0 to 1, with higher values indicating a greater predicted splicing impact.

aa, amino acids; Δ score, delta score; MANE, Matched Annotation from NCBI and EMBL-EBI; SAI-10k-calc, SpliceAI-10k calculator.

Splice site strength was also estimated with MaxEntScan using the GeneBe MaxEntScan Visualizer (Java reimplementation) [27]. MaxEntScan is a bioinformatic tool that uses the Maximum Entropy principle to predict and evaluate 5' donor and 3' acceptor splice sites by analyzing sequence position dependencies. It outputs a MaxEntScore for given sequences, where higher values indicate a greater probability of functioning as a valid splice site. By comparing reference and altered sequences, one can determine how

genetic variants might weaken, abolish, or create new cryptic splice sites. However, because it is only a predictive model, MaxEntScan results should always be interpreted alongside other computational tools and experimental evidence. The tool is freely available online [27] and is based on the MaxEntScan algorithm of Yeo and Burge [28]. The wild-type DNA sequence was entered as 5'-CTCAGCAACTTCTCATGTCTGTAGGTCCTGGCAAATGTAGCCTA-3' and the mutant DNA sequence was entered as 5'-CCTCAGCAACTTCTCATGTCTGGAGGTCCTGGCAAATGTAGCCTA-3'. 3′ss scores were calculated with a 23-bp window (20 bp intron/3 bp exon) and 5′ss scores with a 9-bp window (3 bp exon/6 bp intron), by comparing 45-nt wild-type and mutant sequences centered on the variant. The results obtained on the website showed the following. The variant in the *GPR107* gene c.1132-3T>G lies within the polypyrimidine tract at position −3 of the 3′ splice site, immediately upstream of the invariant AG dinucleotide. The wild-type acceptor site obtained a score of approximately +8, consistent with a functional 3′ splice site. The variant reduced this score by 12.3 points (to approximately −4), indicating a severe loss of acceptor site strength. Scanning of the surrounding sequence did not identify any newly created acceptor or donor site with a positive score in the mutant allele; the apparent score increases at neighboring positions were confined to strongly negative values and are unlikely to be biologically relevant. A weak donor-like motif (GTAGGT, score ≈ +2) overlapping the variant was also disrupted (Δ = −7.6). Together, these predictions suggest that c.1132-3T>G impairs recognition of the canonical intron-exon boundary, which may lead to exon skipping or use of a cryptic splice site (Figure *9*).

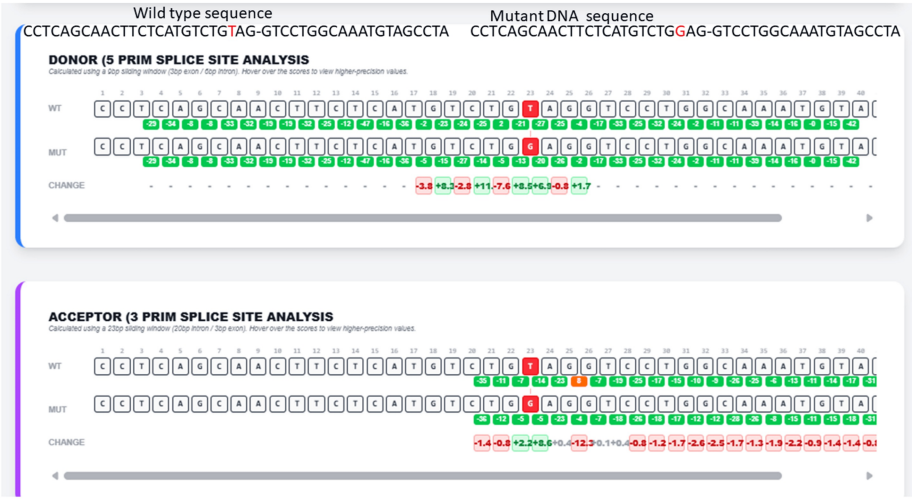



**FIGURE 9: In silico splice-site prediction analysis using MaxEntScan for the GPR107 c.1132-3T>G variant**

MaxEntScan prediction for *GPR107* c.1132-3T>G. Donor (5′ss, 9-bp window) and acceptor (3′ss, 23-bp window) scores for the wild-type (WT) and mutant (MUT) sequences. The variant position is highlighted in red. Numbers below each nucleotide are MaxEntScan scores for the window at that position (green, negative values; orange, positive values). The CHANGE row shows MUT minus WT (red, decrease; green, increase; gray, negligible change). The variant reduces the canonical acceptor score from about +8 to about −4 (Δ = −12.3) and weakens an overlapping donor-like motif (Δ = −7.6), without creating a new splice site.

Thus, we proposed that the fetus was affected by an autosomal recessive genetic disease possibly due to a homozygous loss-of-function near-splice mutation in the *GPR107* gene. Immune hydrops was ruled out by a normal direct Coombs test and normal fetal hemoglobin levels. The lady's blood group was B, Rh-positive. TORCH infections (toxoplasmosis, rubella, cytomegalovirus, and herpes simplex virus) were ruled out by PCR on the amniotic fluid extracted after amniocentesis. Alpha thalassemia was ruled out by normal deletion/duplication analysis of the *HBA1* and *HBA2* genes in the fetus and parents using the multiplex ligation-dependent probe amplification method (MLPA). These investigations follow the recommended diagnostic evaluation for nonimmune hydrops fetalis [29]. The clinical findings, investigations, and genetic results are summarized in Table *1*.

| Category | Findings |
|---|---|
| Family history | Third-degree consanguineous parents; second pregnancy; previous pregnancy with a similarly affected female fetus and in utero death at about 7 months' gestation |
| Parental age | Mother 25 years; father 23 years |
| Antenatal history | No maternal gestational diabetes, pregnancy-induced hypertension, or exposure to teratogenic agents |
| Prenatal ultrasound (second trimester; mean sonographic gestational age 23 weeks) | Hydrops: generalized skin edema, scalp edema, bilateral pleural effusion, ascites. Fetal akinesia/arthrogryposis: hyperextended neck, persistently flexed hips and knees, talipes equinovarus, persistently clenched fists, no spontaneous movements. Amniotic fluid normal (maximum vertical pocket 6.16 cm) |
| Cardiac and other structural anomalies | Two-dimensional fetal echocardiography normal; no other fetal anomalies documented |
| Exclusion of immune hydrops | Direct Coombs test normal; fetal hemoglobin normal; maternal blood group B, Rh-positive |
| Exclusion of congenital infection | TORCH PCR on amniotic fluid negative |
| Exclusion of alpha thalassemia | *HBA1/HBA2* MLPA normal in fetus and parents |
| Chromosomal analysis | Chromosomal microarray normal |
| Trio exome sequencing | Fetus homozygous for *GPR107* NM_020960.5:c.1132-3T>G; both parents heterozygous; variant-caller depth/VAF: fetus 31x/100%, mother 64x/56%, father 54x/48% (Figures 4-6). Fetal DNA from amniotic fluid; parental DNA from EDTA peripheral blood |
| Sanger sequencing | Fetus homozygous; mother and father heterozygous (Figure 7); performed on the same DNA samples used for exome sequencing |
| Variant classification | Variant of uncertain significance (ACMG/AMP: PM2, PP3) |
| Outcome | Termination of pregnancy at 23 weeks; male fetus; hydrops and arthrogryposis multiplex congenita confirmed on examination |

**TABLE 1: Summary of clinical findings, investigations, and genetic results in the present family**

ACMG/AMP, American College of Medical Genetics and Genomics/Association for Molecular Pathology; MLPA, multiplex ligation-dependent probe amplification; PCR, polymerase chain reaction; TORCH, toxoplasmosis, rubella, cytomegalovirus, herpes simplex virus.

Written informed consent was obtained from the patient for publication of this case report; no identifying patient material has been published in this case report. As per our institute policy, no ethics committee approval is needed for publication of a case report.

## Discussion

Orphan GPCRs are seven-transmembrane receptors whose endogenous natural ligands have not yet been conclusively identified or characterized. Despite missing known ligands, several orphan GPCRs are directly linked to single-gene (monogenic) human diseases when mutated, as well as complex conditions. The diseases have been adapted from the Online Mendelian Inheritance in Man (OMIM) database (Table *2*) [30].

| Gene/Receptor | Associated Human Disease/Condition | Clinical Features | Inheritance Pattern |
|---|---|---|---|
| *GPR56 (ADGRG1)* | Bilateral frontoparietal polymicrogyria (BFPP) | Severe developmental delay, intellectual disability, seizures/epilepsy (e.g., Lennox-Gastaut syndrome), cerebellar ataxia, and strabismus due to cortical malformation | Autosomal recessive |
| *GPR68 (OGR1)* | Amelogenesis imperfecta (hypomaturation type 1J) | Severe enamel defects leading to yellow-brown, fragile teeth that break easily; functions as a proton-sensing receptor modulating ameloblast function | Autosomal recessive |
| *GPR88* | Childhood-onset chorea with psychomotor retardation (COCPMR) | Abnormal involuntary movements (chorea), marked speech delay, intellectual disability, and learning difficulties due to impaired striatal signaling | Autosomal recessive |
| *GPR101* | X-Linked acrogigantism (X-LAG) | Extreme early-onset gigantism in infants/toddlers driven by growth hormone (GH) and prolactin hypersecretion, driven by microduplications at Xq26.3 containing *GPR101* leading to early-onset pituitary macroadenomas | X-Linked dominant (often microduplications/de novo) |
| *GPR125 (ADGRA3)* | *GPR125*-related syndromic intellectual disability | Developmental delay, intellectual impairment, microcephaly, and subtle dysmorphic facial features | Autosomal recessive |
| *GPR143 (OA1)* | X-Linked ocular albinism type 1 (OA1) | Congenital nystagmus, reduced visual acuity, foveal hypoplasia, photophobia, and hypopigmentation restricted to the ocular fundus/retinal pigment epithelium (normal hair and skin pigmentation) | X-Linked recessive |
| *GPR161* | Infantile medulloblastoma (Sonic Hedgehog subtype) | Predisposition to SHH-subtype medulloblastoma in early childhood; acts as a negative regulator of the Sonic Hedgehog signaling pathway | Autosomal dominant (germline loss-of-function variants) |
| *GPR179* | Complete congenital stationary night blindness (cCSNB) | Inability to adapt to low light/night blindness, reduced visual acuity, nystagmus, and myopia due to signal transmission defects between photoreceptors and ON-bipolar cells | Autosomal recessive |

**TABLE 2: Orphan GPCRs and associated monogenic human diseases**

Summary of orphan GPCR genes, their corresponding associated human conditions, clinical presentations, and inheritance patterns. Includes *GPR56* (bilateral frontoparietal polymicrogyria), *GPR68* (amelogenesis imperfecta), *GPR88* (childhood-onset chorea with psychomotor retardation), *GPR101* (X-linked acrogigantism), *GPR125* (syndromic intellectual disability), *GPR143* (ocular albinism type 1), *GPR161* (infantile medulloblastoma), and *GPR179* (complete congenital stationary night blindness).

GPCR, G protein-coupled receptor.

Table credit: Original table created independently by the authors using data synthesized from the Online Mendelian Inheritance in Man (OMIM) database [30].

Altered expression of orphan GPCRs plays a critical role in the pathogenesis of various polygenic and complex diseases [31]. In metabolic regulation, receptors such as *GPR21* and *GPR26* are key modulators of energy homeostasis; knockout models demonstrate that disruption of these genes alters glucose tolerance, body weight regulation, and systemic insulin resistance [31]. Within the central nervous system, orphan GPCRs like *GPR6* and *GPR88* are highly enriched in the striatum, where they modulate striatal output and dopaminergic signaling networks, establishing them as promising therapeutic targets for neurodegenerative and neuropsychiatric conditions including Parkinson's disease and schizophrenia [32].

*GPR107,* an orphan GPCR, plays critical roles in intracellular trafficking and embryonic development, initially identified among complementary DNA sequences. Located at chromosome 9q34.2-3, the gene spans 86.4 kb with 18 exons encoding a 552-amino acid protein [5,6,33]. Initially enriched for expression in human lung tissue, and subsequently in the brain, kidney, heart, and liver, it encodes an integral membrane protein localizing in the TGN, suggesting a role in protein trafficking and sorting [7]. It has been demonstrated to act in the endocytosis of extracellular transferrin through CME, essential to cellular iron uptake [7].

Additional functions in general homeostasis include interaction with AT1R (angiotensin II receptor 1) in renal podocyte cells, implying tissue-specific function and expression, with an embryonic study suggesting direct/indirect interaction with a limited number of surface receptors on account of selective deficits in *GPR107* null cells, implying decreased toxin resistance and embryonic viability [34]. The embryonic lethality observed in *Gpr107*-null mice further demonstrates the gene's essential, non-redundant role in development. Although no specific study has confirmed a direct correlation between fetal hydrops formation and *GPR107* mutation/abnormal expression, loss of its function may induce disruption of endocytic pathways/vascular permeability dysfunction, which in turn may induce the condition. A full murine knockout of *Gpr107* displayed homozygous embryonic fatality by mid-gestation (E9.5-E10.5), yolk sac abnormalities including defective vasculogenesis, and a disrupted cubilin-megalin complex formation critical for nutrient transport. It is important to note that this lethal phenotype precludes survival to the equivalent stages where hydrops fetalis typically manifests [8]. *GPR107* null fibroblasts also showed reduced transferrin internalization, resistance to cholera toxin and Pseudomonas exotoxin A and hence retrograde transport, and decreased uptake of low-density lipoprotein receptor-related protein-1 (LRP1) substrate [5,6,33].

Because *GPR107* is an integral membrane protein residing in the TGN that plays a critical role in membrane trafficking and protein sorting, disruptions in closely interacting functional networks frequently underlie prominent human genetic diseases [6]. For instance, mutations in the retromer complex gene *VPS35*, which mediates retrograde transport from endosomes back to the TGN, cause autosomal dominant late-onset Parkinson's disease [35]. Similarly, defects in the multi-subunit Conserved Oligomeric Golgi (COG) tethering complex (*COG1* through *COG8*) disrupt intra-Golgi trafficking and result in severe congenital disorders of glycosylation characterized by multi-system developmental and metabolic abnormalities. Specifically, *COG6* and related deficiencies are well-documented causes of arthrogryposis multiplex congenita driven by early-onset hypotonia and decreased fetal movement [36]. Concurrently, severe phenotypes such as COG7-CDG can present as a lethal congenital disorder due to microcephaly, dysmorphism, hypotonia, cardiac involvement, early lethality, and hepatosplenomegaly, which could present as hydrops fetalis due to multisystem involvement [37]. Furthermore, mutations affecting TGN-localized adaptor protein complexes, such as *AP1S2* and *AP3B1*, impair vesicle formation and cargo delivery to specialized organelles, leading to conditions like X-linked intellectual disability and Hermansky-Pudlak syndrome type 2 [38,39]. Other essential regulatory and structural components operating within this pathway include the guanine nucleotide exchange factor *ARFGEF2*, whose disruption causes periventricular nodular heterotopia and microcephaly due to failed cellular migration during embryonic development, and the Golgi matrix protein *GOLGA2*, where mutations lead to structural fragmentation of the Golgi apparatus, resulting in neuromuscular disorder with microcephaly (Table 3) [40,41].

| Gene(s) | Associated Human Genetic Disease | Clinical Features | Inheritance Pattern |
|---|---|---|---|
| *VPS35* | Parkinson disease 17 (PARK17) | Late-onset motor symptoms (tremor, rigidity, bradykinesia), postural instability, and cognitive decline | Autosomal dominant |
| *COG1-COG8* | Congenital disorders of glycosylation (CDG types II) | Multi-systemic involvement, developmental delay, hypotonia, skeletal abnormalities, and abnormal protein glycosylation profiles | Autosomal recessive |
| *AP1S2* | X-Linked intellectual disability/Pettigrew syndrome | Profound psychomotor retardation, hypotonia, basal ganglia calcification, and Dandy-Walker malformation | X-Linked recessive |
| *AP3B1* | Hermansky-Pudlak syndrome type 2 | Oculocutaneous albinism, bleeding diathesis (platelet storage pool deficiency), and early-onset pulmonary fibrosis | Autosomal recessive |
| *ARFGEF2* | Periventricular nodular heterotopia with microcephaly | Progressive microcephaly, drug-resistant epilepsy, developmental delay, hypotonia, and impaired neuronal migration | Autosomal recessive |
| *GOLGA2* | Golgi fragmentation-related neuromuscular/Developmental disorder | Global developmental delay, muscle weakness, microcephaly, seizures, central hypotonia, and skeletal muscle myopathy | Autosomal recessive |

**TABLE 3: Intracellular trafficking and Golgi-related genes implicated in human genetic disorders**

Overview of intracellular trafficking genes, associated genetic diseases, multisystemic clinical features, and modes of inheritance. Includes *VPS35* (Parkinson disease 17), *COG1-COG8* (congenital disorders of glycosylation type II), *AP1S2* (X-linked intellectual disability/Pettigrew syndrome), *AP3B1* (Hermansky-Pudlak syndrome type 2), *ARFGEF2* (periventricular nodular heterotopia with microcephaly), and *GOLGA2* (Golgi fragmentation-related neuromuscular/developmental disorder).

Table credit: Original table created independently by the authors, synthesized from published clinical literature and OMIM database entries [30,35-41].

In a previous report, we similarly identified a novel homozygous consensus acceptor splice site variant in the *NUP214* gene in a fetus presenting with severe nonimmune hydrops fetalis and fetal akinesia deformation sequence, demonstrating the utility of high-throughput exome sequencing in uncovering novel rare splice variants in fetal lethal phenotypes [42]. Using exome sequencing, we have also previously described a novel consensus acceptor splice site variant in the X-linked *THOC2* gene in two male fetuses with recurrent arthrogryposis multiplex congenita, extending the *THOC2*-related phenotype to a lethal fetal form [43], and a novel homozygous nonsense variant in the *OSBPL9* gene, which encodes a lipid transfer protein acting between the TGN and the endoplasmic reticulum, in a consanguineous family with fetal cerebral ventriculomegaly, cerebellar hypoplasia, and arthrogryposis multiplex [44]. Together with the present case, these reports show that exome sequencing of affected fetuses and their parents can identify new genes and new phenotypes of known genes in fetal akinesia and arthrogryposis.

A protein network analysis using the STRING (Search Tool for Retrieval of Interacting Genes/Proteins) database showed a lack of interactions between *GPR107* and other genes known to be causative for either hydrops fetalis or arthrogryposis multiplex congenita [45]. List of hydrops fetalis genes: *ACAD9, ADAMTS3, AHCY, ALG1, ALG12, ALG8, ALG9, ALPK3, ASAH1, BRAF, BSND, CANT1, CBL, CCBE1, CDAN1, CELSR1, CEP55, CHD7, CHRNA1, CHRND, CHRNG, COG6, COL2A1, CTSA, DHCR24, DHCR7, DNAH9, EBP, ENPP1, EPHB4, FAT4, FGFR3, FIG4, FLT4, FOXC2, FOXP3, FRAS1, FREM2, G6PD, GAA, GALC, GALNS, GATA1, GBA1, GBE1, GLA, GLB1, GLDN, GLUL, GNPTAB, GRIP1, GUSB, HADH, HADHA, HADHB, HBA1, HBA2, HRAS, IDUA, KAT6B, KCNJ1, KCNJ2, KDM6A, KIAA0586, KIF23, KLF1, KLHL40, KMT2D, KRAS, LBR, LIPA, LZTR1, MAP2K1, MAP2K2, MGAT2, MID1, MVK, MYH3, MYOM1, MYRF, NEB, NEK1, NEU1, NEXN, NPC1, NPC2, NRAS, PEX1, PEX10, PEX12, PEX13, PEX14, PEX16, PEX19, PEX2, PEX26, PEX3, PEX5, PEX6, PEX7, PHGDH, PIEZO1, PIGA, PKLR, PMM2, PSAT1, PTH1R, PTPN11, RAF1, RASA1, RIT1, RPL11, RPL15, RPL27, RPL35A, RPL5, RPS10, RPS17, RPS19, RPS24, RPS26, RPS27, RPS29, RPS7, RYR1, SCN5A, SEC23B, SF3B4, SGPL1, SHOC2, SLC12A1, SLC17A5, SLC22A5, SLC26A2, SMPD1, SOS1, SOS2, SOX18, STAT3, SUMF1, SUZ12, TAFAZZIN, TALDO1, TAPT1, TRIP11, UROS, WAC, WDR35, ZEB2* (derived from [46]) (Figure *10*).

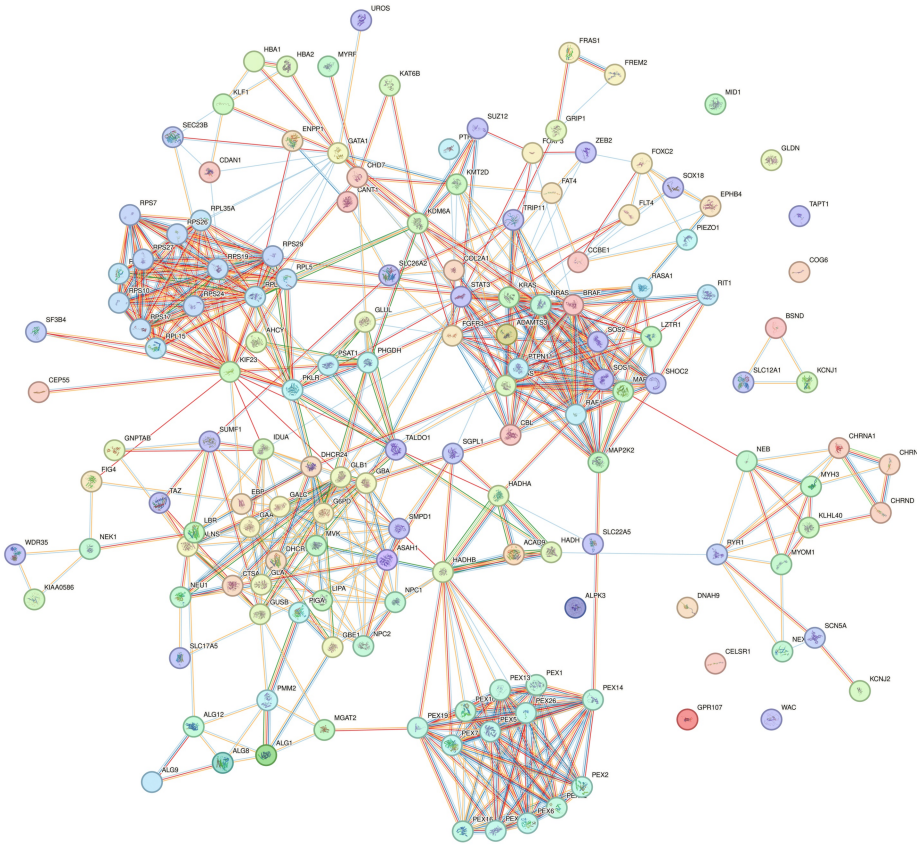



**FIGURE 10: STRING protein interaction network analysis of GPR107 and established hydrops fetalis causative genes**

Protein-protein interaction network generated using the STRING (Search Tool for Retrieval of Interacting Genes/Proteins) database, mapping *GPR107* against a representative, non-exhaustive panel of genes known to be causative for hydrops fetalis. The network demonstrates a distinct lack of physical or functional interactions between *GPR107* (isolated node in the lower right) and established hydrops fetalis-associated gene clusters, suggesting a potentially distinct or novel pathophysiological pathway.

Figure credit: Independently generated by the authors using the STRING database platform [45]. No third-party publisher permission is required as STRING is open access for non-commercial reuse.

List of gene known to cause arthrogryposis: *ACTA1, AGRN, ALG14, ALG2, ALG3, ANTXR2, BICD2, BIN1, CHAT, CHMP1A, CHRNA1, CHRNB1, CHRND, CHRNE, CHRNG, CHST14, CNTN1, CNTNAP1, COL6A1, COL6A2, COL6A3, COLQ, DHCR24, DNM2, DOK7, DPAGT1, ECEL1, EGR2, ERCC1, ERCC5, ERCC6, EXOSC3, FBN1, FBN2, FKBP10, FKRP, FKTN, FLVCR2, GBA, GBE1, GFPT1, GLE1, GMPPB, IGHMBP2, KAT6B, KLHL40, KLHL41, LMNA, LMOD3, LRP4, MAGEL2, MPZ, MTM1, MUSK, MYBPC1, MYH2, MYH3, MYH8, NALCN, NEB, PIEZO2, PIP5K1C, PLOD2, RAPSN, RIPK4, RYR1, SCARF2, SCN4A, SELENON, SKI, SLC35A3, SLC39A13, SLC5A7, SOX10, SYNE1, SYT2, TGFB3, TNNI2, TNNT1, TNNT3, TPM2, TPM3, TRIP4, TRPV4, TSEN54, TTN, UBA1, VIPAS39, VPS33B, ZC4H2* (derived from [47]) (Figure *11*).

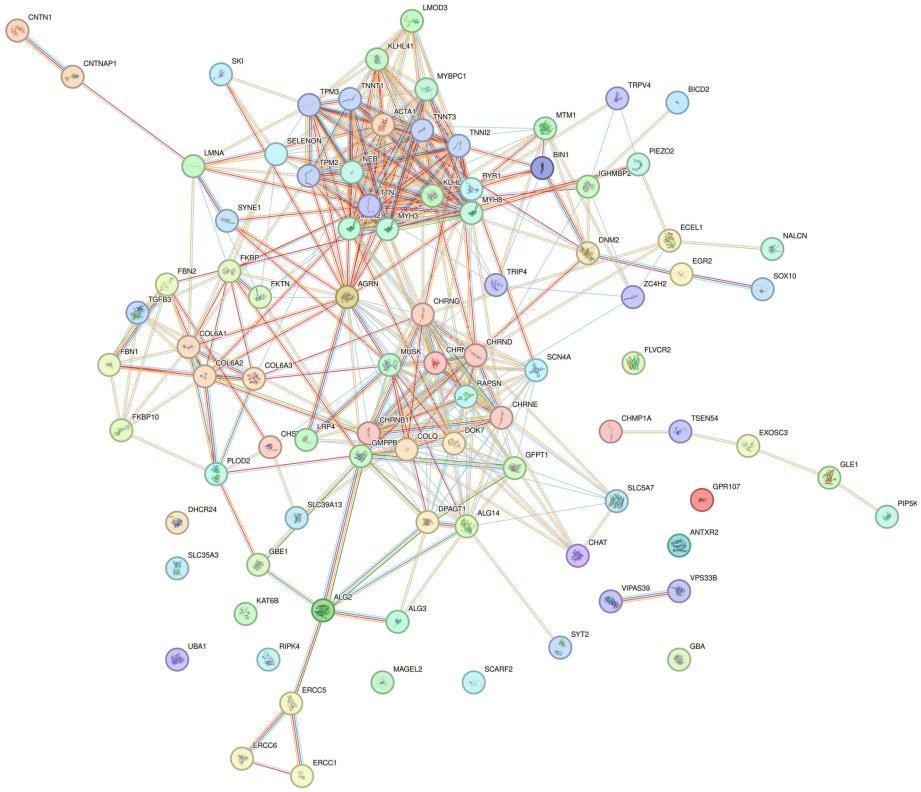



**FIGURE 11: STRING protein interaction network analysis of GPR107 and established arthrogryposis multiplex congenita causative genes**

Protein-protein interaction network generated using the STRING (Search Tool for Retrieval of Interacting Genes/Proteins) database, evaluating *GPR107* against a representative, non-exhaustive panel of genes known to be causative for arthrogryposis multiplex congenita (comprising 90 nodes). The network reveals a distinct lack of physical or functional interactions between *GPR107* (isolated node on the right side) and established arthrogryposis multiplex congenita-associated gene clusters, indicating a potentially distinct molecular mechanism.

Figure credit: Independently generated by the authors using the STRING database platform [45]. No third-party publisher permission is required as STRING is open access for non-commercial reuse.

To help identify further affected families, the variant will be submitted to the ClinVar database [48], and the fetal phenotype has been described above using standardized HPO terms [11].

The family was counselled about the basics of genetics and inheritance mechanisms. They were counselled about the likely recurrence risk of such a disease as 25% in every pregnancy. Prenatal diagnosis will have to rely on fetal USG since this variant is classified as a VUS as per ACMG (American College of Medical Genetics) classification [10]. The other options offered were reproduction using donor gametes (donor sperm or eggs).

### Limitations of the study

The limitations of this study are the lack of RNA or protein studies proving the exact mechanism of pathogenesis of this variant, the lack of detailed autopsy findings, and the lack of DNA study in the previously affected fetus. Reverse transcription-PCR of RNA from fetal tissue or cultured amniocytes, or a minigene splicing assay, would be needed to show the predicted skipping of exon 13 [9]; such studies were not possible in the present study. Because there is no functional evidence and only one family has been studied, the variant remains a VUS under ACMG/AMP criteria [10], and the association between *GPR107* and this phenotype should be regarded as a candidate association rather than an established one.

## Conclusions

Herein, we propose a novel gene-disease association (candidate gene), namely hydrops fetalis with fetal arthrogryposis multiplex congenita, with a *GPR107* gene-predicted loss-of-function variant inherited in an autosomal recessive fashion. This association is not yet established and should be considered provisional until it is confirmed in additional unrelated families and by functional studies. The primary limitation of this

study is the lack of RNA or protein studies proving the exact mechanism of pathogenesis of this variant. Reporting of further such cases is needed to confirm or refute this association. This will aid in accurate genetic counseling and prevention of recurrences in such families in the future using fetal DNA diagnosis or embryonic DNA diagnosis (preimplantation genetic diagnosis).

# Additional Information

## Author Contributions

All authors have reviewed the final version to be published and agreed to be accountable for all aspects of the work.

**Concept and design:** Parag M. Tamhankar, Mandakini Pradhan, Kritika Agnihotri, Vasundhara Tamhankar, Salil Vaniawala, Arnav Asher, Tushar Kachhadiya, Shalin Vaniawala, Pramila Menon, Shwetal Patel

**Acquisition, analysis, or interpretation of data:** Parag M. Tamhankar, Mandakini Pradhan, Kritika Agnihotri, Vasundhara Tamhankar, Salil Vaniawala, Arnav Asher, Tushar Kachhadiya, Shalin Vaniawala, Pramila Menon, Shwetal Patel

**Drafting of the manuscript:** Parag M. Tamhankar, Mandakini Pradhan, Kritika Agnihotri, Vasundhara Tamhankar, Salil Vaniawala, Arnav Asher, Tushar Kachhadiya, Shalin Vaniawala, Pramila Menon, Shwetal Patel

**Critical review of the manuscript for important intellectual content:** Parag M. Tamhankar, Mandakini Pradhan, Kritika Agnihotri, Vasundhara Tamhankar, Salil Vaniawala, Arnav Asher, Tushar Kachhadiya, Shalin Vaniawala, Pramila Menon, Shwetal Patel

**Supervision:** Parag M. Tamhankar, Mandakini Pradhan, Salil Vaniawala

## Disclosures

**Human subjects:** Informed consent for treatment and open access publication was obtained or waived by all participants in this study. **Conflicts of interest:** In compliance with the ICMJE uniform disclosure form, all authors declare the following: **Payment/services info:** All authors have declared that no financial support was received from any organization for the submitted work. **Financial relationships:** Arnav Asher declare(s) non-financial support from Centre for Medical Genetics, Mumbai, India. He worked as a voluntary research assistant on this project and is not an employee of either Centre for Medical Genetics or SN Gene Lab Pvt Ltd. The diagnostic testing and analysis were conducted as part of routine clinical services or academic case review, and no external commercial funding or sponsorship was received for the preparation or publication of this manuscript. The authors declare no other competing financial or personal interests. Shwetal Patel declare(s) employment from SN Gene Lab Pvt Ltd, Surat, India. She is an employee of SN Gene Lab Pvt Ltd and contributed to genetic analysis, bioinformatics, data collection, and manuscript preparation. The diagnostic testing and analysis were conducted as part of routine clinical services or academic case review, and no external commercial funding or sponsorship was received for the preparation or publication of this manuscript. The authors declare no other competing financial or personal interests. Shalin Vaniawala declare(s) stock/stock options from SN Gene Lab Pvt Ltd, Surat, India. He is a co-Director of SN Gene Lab Pvt Ltd and is also attached as a Medical Officer to the same institute. He contributed to genetic analysis, data collection, and manuscript preparation. The diagnostic testing and analysis were conducted as part of routine clinical services or academic case review, and no external commercial funding or sponsorship was received for the preparation or publication of this manuscript. The authors declare no other competing financial or personal interests. Salil Vaniawala declare(s) stock/stock options from SN Gene Lab Pvt Ltd. He is a Director of SN Gene Lab Pvt Ltd and also the Chief Geneticist at the same institute. He supervised the project and guided in genetic analysis, data collection, and manuscript preparation. The diagnostic testing and analysis were conducted as part of routine clinical services or academic case review, and no external commercial funding or sponsorship was received for the preparation or publication of this manuscript. The authors declare no other competing financial or personal interests. Vasundhara Tamhankar declare(s) employment from SN Gene Lab Pvt Ltd. She works as a Consultant Medical Geneticist at SN Gene Lab Pvt Ltd. She helped with genetic analysis, data collection, and manuscript preparation. The diagnostic testing and analysis were conducted as part of routine clinical services or academic case review, and no external commercial funding or sponsorship was received for the preparation or publication of this manuscript. The authors declare no other competing financial or personal interests. Parag M Tamhankar declare(s) employment from SN Gene Lab Pvt Ltd. He works as a Consultant Medical Geneticist at SN Gene Lab Pvt Ltd. He supervised the project, helped in genetic analysis, bioinformatic analysis, and manuscript preparation. The diagnostic testing and analysis were conducted as part of routine clinical services or academic case review, and no external commercial funding or sponsorship was received for the preparation or publication of this manuscript. The authors declare no other competing financial or personal interests. Tushar Kachhadiya declare(s) employment from SN Gene Lab Pvt Ltd, Surat, India. He is an employee of SN Gene Lab Pvt Ltd and contributed to genetic analysis, bioinformatics, data collection, and manuscript preparation. The diagnostic testing and analysis were conducted as part of routine clinical services or academic case

review, and no external commercial funding or sponsorship was received for the preparation or publication of this manuscript. The authors declare no other competing financial or personal interests. **Other relationships:** All authors have declared that there are no other relationships or activities that could appear to have influenced the submitted work.

## Acknowledgements

The authors would like to thank the patient's family for sharing their novel case findings and their consent for publication of this report. The authors would also like to thank the staff of the Department of Fetal Medicine, Sanjay Gandhi Postgraduate Institute for Medical Sciences, for their assistance in managing this patient. We would also like to thank the staff of the Centre for Medical Genetics, Mrs. Dipti Mestry, Mrs. Rakhi Kesarkar, and Miss Gungun Parmar for their secretarial assistance and project coordination. AI Disclosure: Generative AI tools (Claude, Anthropic, San Francisco, CA, USA; Gemini, Google LLC, Mountain View, CA, USA) were utilized solely for grammar editing, stylistic refinement, and language polishing during manuscript preparation. The authors authored, reviewed, and verified all scientific content, medical interpretations, bioinformatic data, and references.

# References

1. Niles KM, Blaser S, Shannon P, Chitayat D: Fetal arthrogryposis multiplex congenita/fetal akinesia deformation sequence (FADS)-Aetiology, diagnosis, and management. Prenat Diagn. 2019, 39:720-31. 10.1002/pd.5505
2. Filges I, Hall JG: Failure to identify antenatal multiple congenital contractures and fetal akinesia--Proposal of guidelines to improve diagnosis. Prenat Diagn. 2013, 33:61-74. 10.1002/pd.4011
3. Vanaparthy R, Vadakekut ES, Mahdy H: Nonimmune hydrops fetalis. StatPearls [Internet]. StatPearls Publishing, Treasure Island, FL; 2024.
4. Mastromoro G, Guadagnolo D, De Luca A, Rongioletti MC, Pizzuti A: Fetal hydrops: Genetic dissection of an unspecific sonographic finding-A comprehensive review. Diagnostics (Basel). 2025, 15:465. 10.3390/diagnostics15040465
5. Edgar AJ: Human GPR107 and murine Gpr108 are members of the LUSTR family of proteins found in both plants and animals, having similar topology to G-protein coupled receptors. DNA Seq. 2007, 18:235-41. 10.1080/10425170701207182
6. Tafesse FG, Guimaraes CP, Maruyama T, Carette JE, Lory S, Brummelkamp TR, Ploegh HL: GPR107, a G-protein-coupled receptor essential for intoxication by Pseudomonas aeruginosa exotoxin A, localizes to the Golgi and is cleaved by furin. J Biol Chem. 2014, 289:24005-18. 10.1074/jbc.M114.589275
7. Zhou GL, Na SY, Niedra R, Seed B: Deficits in receptor-mediated endocytosis and recycling in cells from mice with Gpr107 locus disruption. J Cell Sci. 2014, 127:3916-27. 10.1242/jcs.135269
8. The Jackson Laboratory. Gpr107-null mice, strain #032822 (B6.129S6-Gpr107tm1Brs/J). (2026). Accessed: October 8, 2026: https://www.jax.org/strain/032822.
9. Walker LC, Hoya M, Wiggins GA, et al.: Using the ACMG/AMP framework to capture evidence related to predicted and observed impact on splicing: Recommendations from the ClinGen SVI Splicing Subgroup. Am J Hum Genet. 2023, 110:1046-67. 10.1016/j.ajhg.2023.06.002
10. Richards S, Aziz N, Bale S, et al.: Standards and guidelines for the interpretation of sequence variants: A joint consensus recommendation of the American College of Medical Genetics and Genomics and the Association for Molecular Pathology. Genet Med. 2015, 17:405-24. 10.1038/gim.2015.30
11. Köhler S, Gargano M, Matentzoglu N, et al.: The human phenotype ontology in 2021. Nucleic Acids Res. 2021, 49:D1207-17. 10.1093/nar/gkaa1043
12. Broad Institute: HaplotypeCaller. GATK Documentation . (2026). Accessed: October 8, 2026: https://gatk.broadinstitute.org/hc/en-us/articles/360037225632-HaplotypeCaller.
13. Plagnol V, Curtis J, Epstein M, et al.: A robust model for read count data in exome sequencing experiments and implications for copy number variant calling. Bioinformatics. 2012, 28:2747-54. 10.1093/bioinformatics/bts526
14. International Genome Sample Resource: 1000 Genomes Project . (2026). Accessed: October 8, 2026: https://www.internationalgenome.org/.
15. Exome Aggregation Consortium. ExAC Browser . (2026). Accessed: October 8, 2026: https://gnomad.broadinstitute.org/downloads#exac-variants.
16. Broad Institute: gnomAD: Genome Aggregation Database . (2026). Accessed: October 8, 2026: https://gnomad.broadinstitute.org/.
17. National Center for Biotechnology Information: dbSNP: Short Genetic Variations . (2026). Accessed: October 8, 2026: https://www.ncbi.nlm.nih.gov/snp/.
18. Harvard University: PolyPhen-2: Prediction of Functional Effects of Human nsSNPs . (2026). Accessed: October 8, 2026: http://genetics.bwh.harvard.edu/pph2/.
19. J. Craig Venter Institute. SIFT: Sorting Intolerant From Tolerant . (2026). Accessed: October 8, 2026: https://siftdna.org/.
20. Charité - Universitätsmedizin Berlin: MutationTaster. Mutation Tasting . (2026). Accessed: October 8, 2026: https://www.mutationtaster.org/.
21. Sanger F, Nicklen S, Coulson AR: DNA sequencing with chain-terminating inhibitors. Proc Natl Acad Sci U S A. 1977, 74:5463-7. 10.1073/pnas.74.12.5463
22. Franklin by Qiagen. The Future of Genomic Medicine . (2026). Accessed: October 8, 2026: https://franklin.genoox.com/.
23. Broad Institute: SpliceAI Lookup . (2026). Accessed: October 8, 2026: https://spliceailookup.broadinstitute.org/.
24. Jaganathan K, Kyriazopoulou Panagiotopoulou S, McRae JF, et al.: Predicting splicing from primary

sequence with deep learning. Cell. 2019, 176:535-548.e24. 10.1016/j.cell.2018.12.015
25. Zeng T, Li YI: Predicting RNA splicing from DNA sequence using Pangolin . Genome Biol. 2022, 23:103. 10.1186/s13059-022-02664-4
26. Canson DM, Davidson AL, de la Hoya M, Parsons MT, Glubb DM, Kondrashova O, Spurdle AB: SpliceAI-10k calculator for the prediction of pseudoexonization, intron retention, and exon deletion. Bioinformatics. 2023, 39:btad179. 10.1093/bioinformatics/btad179
27. GeneBe: MaxEntScan Visualize . (2026). Accessed: October 8, 2026: https://genebe.net/tools/maxentscan.
28. Yeo G, Burge CB: Maximum entropy modeling of short sequence motifs with applications to RNA splicing signals. J Comput Biol. 2004, 11:377-94. 10.1089/1066527041410418
29. Norton ME, Chauhan SP, Dashe JS: Society for maternal-fetal medicine (SMFM) clinical guideline #7: Nonimmune hydrops fetalis. Am J Obstet Gynecol. 2015, 212:127-39. 10.1016/j.ajog.2014.12.018
30. McKusick-Nathans Institute of Genetic Medicine, Johns Hopkins University: Online Mendelian Inheritance in Man, OMIM. (2026). Accessed: October 8, 2026: https://omim.org/.
31. Davenport AP, Alexander SP, Sharman JL, et al.: International Union of Basic and Clinical Pharmacology. LXXXVIII. G protein-coupled receptor list: Recommendations for new pairings with cognate ligands. Pharmacol Rev. 2013, 65:967-86. 10.1124/pr.112.007179
32. Komatsu H: Novel therapeutic GPCRs for psychiatric disorders . Int J Mol Sci. 2015, 16:14109-21. 10.3390/ijms160614109
33. Yosten GL, Redlinger LJ, Samson WK: Evidence for an interaction of neuronostatin with the orphan G protein-coupled receptor, GPR107. Am J Physiol Regul Integr Comp Physiol. 2012, 303:R941-9. 10.1152/ajpregu.00336.2012
34. Xu D, Tong Z, Yang P, et al.: G protein-coupled receptor 107 deficiency promotes development of diabetic nephropathy. Mol Biomed. 2025, 6:10. 10.1186/s43556-025-00250-1
35. Vilariño-Güell C, Wider C, Ross OA, et al.: VPS35 mutations in Parkinson disease . Am J Hum Genet. 2011, 89:162-7. 10.1016/j.ajhg.2011.06.001
36. Cirnigliaro L, Bianchi P, Sturiale L, et al.: COG6-CDG: Novel variants and novel malformation . Birth Defects Res. 2022, 114:165-74. 10.1002/bdr2.1981
37. Wu X, Steet RA, Bohorov O, et al.: Mutation of the COG complex subunit gene COG7 causes a lethal congenital disorder. Nat Med. 2004, 10:518-23. 10.1038/nm1041
38. Tarpey PS, Stevens C, Teague J, et al.: Mutations in the gene encoding the Sigma 2 subunit of the adaptor protein 1 complex, AP1S2, cause X-linked mental retardation. Am J Hum Genet. 2006, 79:1119-24. 10.1086/510137
39. Dell'Angelica EC, Shotelersuk V, Aguilar RC, Gahl WA, Bonifacino JS: Altered trafficking of lysosomal proteins in Hermansky-Pudlak syndrome due to mutations in the beta 3A subunit of the AP-3 adaptor. Mol Cell. 1999, 3:11-21. 10.1016/S1097-2765(00)80170-7
40. Sheen VL, Ganesh VS, Topcu M, et al.: Mutations in ARFGEF2 implicate vesicle trafficking in neural progenitor proliferation and migration in the human cerebral cortex. Nat Genet. 2004, 36:69-76. 10.1038/ng1276
41. Shamseldin HE, Bennett AH, Alfadhel M, Gupta V, Alkuraya FS: GOLGA2, encoding a master regulator of golgi apparatus, is mutated in a patient with a neuromuscular disorder. Hum Genet. 2016, 135:245-51. 10.1007/s00439-015-1632-8
42. Tamhankar V, Patel SJ, Kachhadiya T, et al.: The first case report of a homozygous consensus acceptor splice variant in the NUP214 gene associated with fetal hydrops and arthrogryposis multiplex. Cureus. 2024, 16:e73252. 10.7759/cureus.73252
43. Tamhankar V, Tamhankar P, Chaubal R, Chaubal J, Chaubal N: Novel consensus splice site pathogenic variation in THOC2 gene leads to recurrent arthrogryposis multiplex congenita phenotype: A case report. Cureus. 2021, 13:e19682. 10.7759/cureus.19682
44. Tamhankar PM, Kachhadiya T, Tamhankar V, Menon PG, Vaniawala S, Mithbawkar SM: The first known case report of a novel homozygous nonsense variant in the OSBPL9 gene associated with fetal cerebral ventriculomegaly, cerebellar hypoplasia, and arthrogryposis multiplex. Cureus. 2025, 17:e80010. 10.7759/cureus.80010
45. STRING Consortium. STRING: Functional Protein Association Networks . (2026). Accessed: October 8, 2026: https://string-db.org.
46. PreventionGenetics: Non-immune Hydrops Fetalis Panel (Test Code 12661) . (2026). Accessed: October 8, 2026: https://www.preventiongenetics.com/tests/non-immune-hydrops-fetalis-panel.
47. GeneDx: Arthrogryposis Panel (Test Code 1119). (2026). Accessed: October 8, 2026: https://providers.genedx.com/tests.
48. Landrum MJ, Chitipiralla S, Brown GR, et al.: ClinVar: Improvements to accessing data. Nucleic Acids Res. 2020, 48:D835-44. 10.1093/nar/gkz972